### Title

Joint effects of genes underlying a temperature specialization tradeoff in yeast




### Journal

PLOS Genetics, 17(9)

### ISSN

1553-7390



### Authors

AlZaben, Faisal
Chuong, Julie N
Abrams, Melanie B
et al.



### Publication Date

2021

### DOI

10.1371/journal.pgen.1009793

PLOS GENETICS

RESEARCH ARTICLE

# Joint effects of genes underlying a temperature specialization tradeoff in yeast

**Faisal AlZaben**[¤a], **Julie N. Chuong**[¤b], **Melanie B. Abrams**, **Rachel B. Brem***

Department of Plant and Microbial Biology, UC Berkeley, Berkeley, California, United States of America

¤a Current address: Ph.D. Program in Molecules, Cells, and Organisms, Harvard University, Boston, Massachusetts, United States of America
¤b Current address: Ph.D. Program in Biology, New York University, New York, New York, United States of America
* rbrem@berkeley.edu





**Citation:** AlZaben F, Chuong JN, Abrams MB, Brem RB (2021) Joint effects of genes underlying a temperature specialization tradeoff in yeast. PLoS Genet 17(9): e1009793. https://doi.org/10.1371/journal.pgen.1009793

**Editor:** Justin C. Fay, University of Rochester, UNITED STATES

**Received:** March 4, 2021

**Accepted:** August 26, 2021

**Published:** September 14, 2021



**Data Availability Statement:** All relevant data are within the manuscript or at Dryad: https://doi.org/10.6078/D11M7F.

**Funding:** This work was supported by NIH R01 GM120430 to R.B.B. and NSF GRFP DGE 1752814 to M.B.A. The funders had no role in study design, data collection and analysis, decision to publish, or preparation of the manuscript.

**Competing interests:** The authors have declared that no competing interests exist.

## Abstract

A central goal of evolutionary genetics is to understand, at the molecular level, how organisms adapt to their environments. For a given trait, the answer often involves the acquisition of variants at unlinked sites across the genome. Genomic methods have achieved landmark successes in pinpointing these adaptive loci. To figure out how a suite of adaptive alleles work together, and to what extent they can reconstitute the phenotype of interest, requires their transfer into an exogenous background. We studied the joint effect of adaptive, gain-of-function thermotolerance alleles at eight unlinked genes from *Saccharomyces cerevisiae*, when introduced into a thermosensitive sister species, *S. paradoxus*. Although the loci damped each other's beneficial impact (that is, they were subject to negative epistasis), most boosted high-temperature growth alone and in combination, and none was deleterious. The complete set of eight genes was sufficient to confer ~15% of the *S. cerevisiae* thermotolerance phenotype in the *S. paradoxus* background. The same loci also contributed to a heretofore unknown advantage in cold growth by *S. paradoxus*. Together, our data establish temperature resistance in yeasts as a model case of a genetically complex evolutionary tradeoff, which can be partly reconstituted from the sequential assembly of unlinked underlying loci.

## Author summary

Organisms adapt to threats in the environment by acquiring DNA sequence variants that tweak traits to improve fitness. Experimental studies of this process have proven to be a particular challenge when they involve manipulation of a suite of genes, all on different chromosomes. We set out to understand how so many loci could work together to confer a trait. We used as a model system eight genes that govern the ability of the unicellular yeast *Saccharomyces cerevisiae* to grow at high temperature. We introduced these variant loci stepwise into a non-thermotolerant sister species, and found that the more *S. cerevisiae* alleles we added, the better the phenotype. We saw no evidence for toxic interactions between the genes as they were combined. We also used the eight-fold transgenic to

dissect the biological mechanism of thermotolerance. And we discovered a tradeoff: the same alleles that boosted growth at high temperature eroded the organism's ability to deal with cold conditions. These results serve as a case study of modular construction of a trait from nature, by assembling the genes together in one genome.

## Introduction

Understanding how organisms acquire new traits is a driving question in evolutionary biology. Many traits of interest are adaptations, meaning they provide a fitness benefit to the organism which has driven their rise to high frequency in the population. Genomic methods often find a slew of unlinked changes at the DNA level that associate with a given adaptive trait [1–4]. For any one candidate locus, gold-standard validation experiments will then swap alleles between taxa and test for an impact on phenotype, at genic [5–10] and sub-genic [11–20] levels of resolution. Though elegant and rigorous, this focused approach on a single gene at a time will by necessity leave polygenic mechanisms of the trait less well characterized.

For a more complete picture of a complex adaptation, we would establish how multiple underlying genes work together, including their interdependence and their joint ability to recapitulate the phenotype. Such questions have come within reach in laboratory evolution, with particular emphasis on genomic methods to infer evidence for epistasis between unlinked adaptive loci [7,21–29]. In a handful of cases, adaptive multi-gene interactions from a lab evolution have been verified experimentally by allelic replacement [30,31]. To date, validating these principles in the context of evolution from the wild has posed a key challenge (although see [32–34]).

To study complex genetic mechanisms in adaptation, we set out to use natural variation in *Saccharomyces* yeasts as a model. *S. cerevisiae* strains, from the wild and the lab, grow at temperatures up to 41˚C [35–37]. All other species in the *Saccharomyces* clade, which diverged from a common ancestor ~20 million years ago, grow poorly at high temperatures, though many outperform *S. cerevisiae* in the cold [38]. In previous work [39] we developed a genomic version of the reciprocal hemizygosity test to dissect thermotolerance, using *S. paradoxus*, the closest sister species to *S. cerevisiae*, as a representative of the inferred ancestral state. Derived alleles of the mapped genes in *S. cerevisiae*, when tested individually for their marginal effects, were partially necessary or sufficient for thermotolerance, or both [39], and their sequences exhibit evidence for positive selection in *S. cerevisiae* [39,40]. But how these genes work together has remained unknown. We thus aimed to investigate the extent to which unlinked thermotolerance loci assembled in the same background would explain the trait, and whether and how these genes would depend on one another for their effects. We expected that any answers could also help elucidate other facets of the mechanism and the evolutionary history of thermotolerance.

## Results

### Combining thermotolerance loci to reconstitute a complex trait

We previously mapped eight genes with pro-thermotolerance alleles in *S. cerevisiae* (Table 1; [39]). To explore the joint function of these unlinked loci, we introduced the alleles of all eight from DBVPG1373, a soil isolate of *S. cerevisiae* from the Netherlands, into Z1, a strain of the sister species *S. paradoxus*, isolated from an English oak tree [41]. Our approach used a stepwise set of gene replacements. With CRISPR/Cas9 we introduced the *S. cerevisiae* allele of the

**Table 1. Genes contributing to thermotolerance divergence between *Saccharomyces cerevisiae* and *S. paradoxus*.** GO, Gene Ontology biological process. The last column reports amino acid divergence between *S. cerevisiae* DBVPG1373 and *S. paradoxus* Z1.

| Gene | GO terms | Location | Description | Protein Length (residues) | Protein Identity (%) |
|---|---|---|---|---|---|
| *AFG2/ YLR397C* | ribosomal large subunit biogenesis | Ch. XII 912550–914892 | Essential for pre-60S maturation and release of several pre-ribosome maturation factors | 780 | 93.6 |
| *APC1/ YNL172W* | mitotic cell cycle | Ch. XIV 310636–315882 | Largest subunit of the Anaphase-Promoting Complex; a ubiquitin-protein ligase required for degradation of anaphase inhibitors | 1748 | 90.6 |
| *CEP3/ YMR168C* | mitotic cell cycle | Ch. XIII 597332–599158 | Essential kinetochore protein; component of the CBF3 complex that binds the CDEIII region of the centromere | 575 | 93.2 |
| *DYN1/ YKR054C* | mitotic cell cycle | Ch. XI 535647–547925 | Heavy chain dynein; microtubule motor protein; required for anaphase spindle elongation | 4092 | 87.5 |
| *ESP1/ YGR098C* | mitotic cell cycle | Ch. VII 682566–687458 | Separase/separin; aids in the dislocation of cohesin from chromatin and sister chromatin segregation | 1630 | 89.9 |
| *MYO1/ YHR023W* | mitotic cell cycle | Ch. VIII 151666–157452 | Type II myosin heavy chain; required for cytokinesis and cell separation | 1928 | 91.9 |
| *SCC2/ YDR180W* | mitotic cell cycle | Ch. IV 821295–825776 | A complex required for loading of cohesin complexes onto chromosomes; involved in establishing sister chromatid cohesion during DSB repair via histone H2AX; subunit of cohesin loading factor (Scc2p-Scc4p) | 1493 | 88.2 |
| *TAF2/ YCR042C* | chromatin binding | Ch. III 201174–205397 | TFIID subunit; involved in RNA polymerase II transcription initiaition | 1407 | 89.8 |

https://doi.org/10.1371/journal.pgen.1009793.t001

promoter and coding region of a given gene into the endogenous location in wild-type *S. paradoxus*; we used the resulting strain as a background for the replacement of the *S. paradoxus* allele of the next gene by that of *S. cerevisiae*; and so on until all eight genes were swapped into one genome (Fig 1, bottom).

We first assayed growth of the eight-gene transgenic and the wild-type parental species at high temperature, with biomass accumulation (growth efficiency; the increase in optical density after 24 hours relative to that at the start) as a readout of strain performance. The results revealed an advantage of 2.07-fold attributable to the eight *S. cerevisiae* alleles in the *S. paradoxus* background at 39˚C (Fig 1, inset and S1A Table), and no such effect in 28˚C control conditions (S1 Fig). This joint phenotype recapitulated 15% of the trait divergence between wild-type *S. cerevisiae* and *S. paradoxus* at 39˚C (Fig 1, inset), with predictive power tailing off near 37˚C (S2 Fig). These data make clear that even at 39˚C, the full genetic architecture of *S. cerevisiae* thermotolerance must involve more loci than the eight we have manipulated here—highlighting the potential for high genetic complexity of this trait divergence between species.

## Negative epistasis among thermotolerance genes

We hypothesized that *S. cerevisiae* thermotolerance determinants might depend on one another to confer their effects. We sought to test this at the whole-gene level, treating the allele of each thermotolerance locus (including the promoter and coding region) as a module, and investigating the interactions between them. The *S. cerevisiae* allele of each module, when introduced on its own into *S. paradoxus*, was sufficient for a <1.4-fold benefit in biomass accumulation at 39˚C, as expected (S3 Fig and [39]). We summed these measurements to yield an expected phenotype under the assumption of independent gene function, which we compared

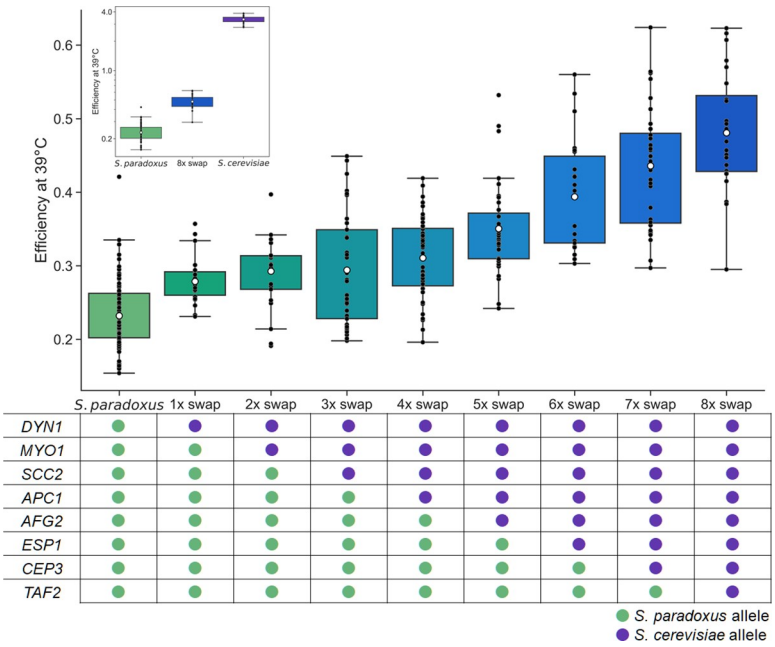


**Fig 1. *S. cerevisiae* alleles of thermotolerance loci jointly improve growth at high temperature.** In each plot, the *y*-axis reports growth efficiency at 39˚C, the cell density after a 24-hour incubation as a difference from the starting density. In the main plot, each column reports data from a transgenic *S. paradoxus* strain harboring *S. cerevisiae* alleles of the indicated thermotolerance loci, or the wild-type *S. paradoxus* progenitor. At bottom, each cell reports the genotype at the indicated locus in the indicated strain. The inset shows purebred wild-types and the *S. paradoxus* strain harboring all eight thermotolerance loci from *S. cerevisiae* (8x swap); the *y*-axis is log-scaled. Black points report individual biological replicates and white dots report means. Boxes span the interquartile range. Whiskers are 1.5 times the interquartile range. Statistical analyses are reported in S1A Table.

https://doi.org/10.1371/journal.pgen.1009793.g001

to the true measurement from the *S. paradoxus* strain harboring all eight thermotolerance loci from *S. cerevisiae*. The latter came in significantly below the estimate from the model assuming independence (Fig 2A). Thus, the combination of all eight genes was subject to negative epistasis, improving growth at high temperature to an extent less than the sum of its parts.

We next turned to the strains we had made in the service of the eight-gene transgenic. These harbored *S. cerevisiae* modules of one thermotolerance gene in the *S. paradoxus* background, two genes, three genes, and so on (Fig 1, bottom). We considered this strain panel as an arbitrary trajectory through a gene-wise genetic landscape from the *S. paradoxus* wild-type to the eight-locus swap. Though it represented just one of tens of thousands of possible paths to the eight-fold transgenic genotype, we anticipated that it could help inform our understanding of the genetic architecture of thermotolerance.

In assays of biomass accumulation at 39˚C in each strain of the panel, we saw a generally monotonic relationship between thermotolerance and the number of *S. cerevisiae* gene modules introduced into *S. paradoxus* (Fig 1 and S1A Table). No such pattern emerged from a 28˚C control (S1 Fig and S1B Table). For a quantitative analysis, we converted the phenotypic profiles in the strain set to effect sizes, each reporting the impact of the *S. cerevisiae* allele of a gene on thermotolerance, in the chimeric background into which it was introduced (Fig 2B). Inspection of this metric confirmed that each *S. cerevisiae* gene addition boosted the phenotype along the path to the eight-fold transgenic, in most cases significantly so (S1A Table), with one exception. The pro-thermotolerance function of *S. cerevisiae SCC2* (encoding a cohesin loading factor), discernable when it was introduced on its own into *S. paradoxus* (S3 Fig),

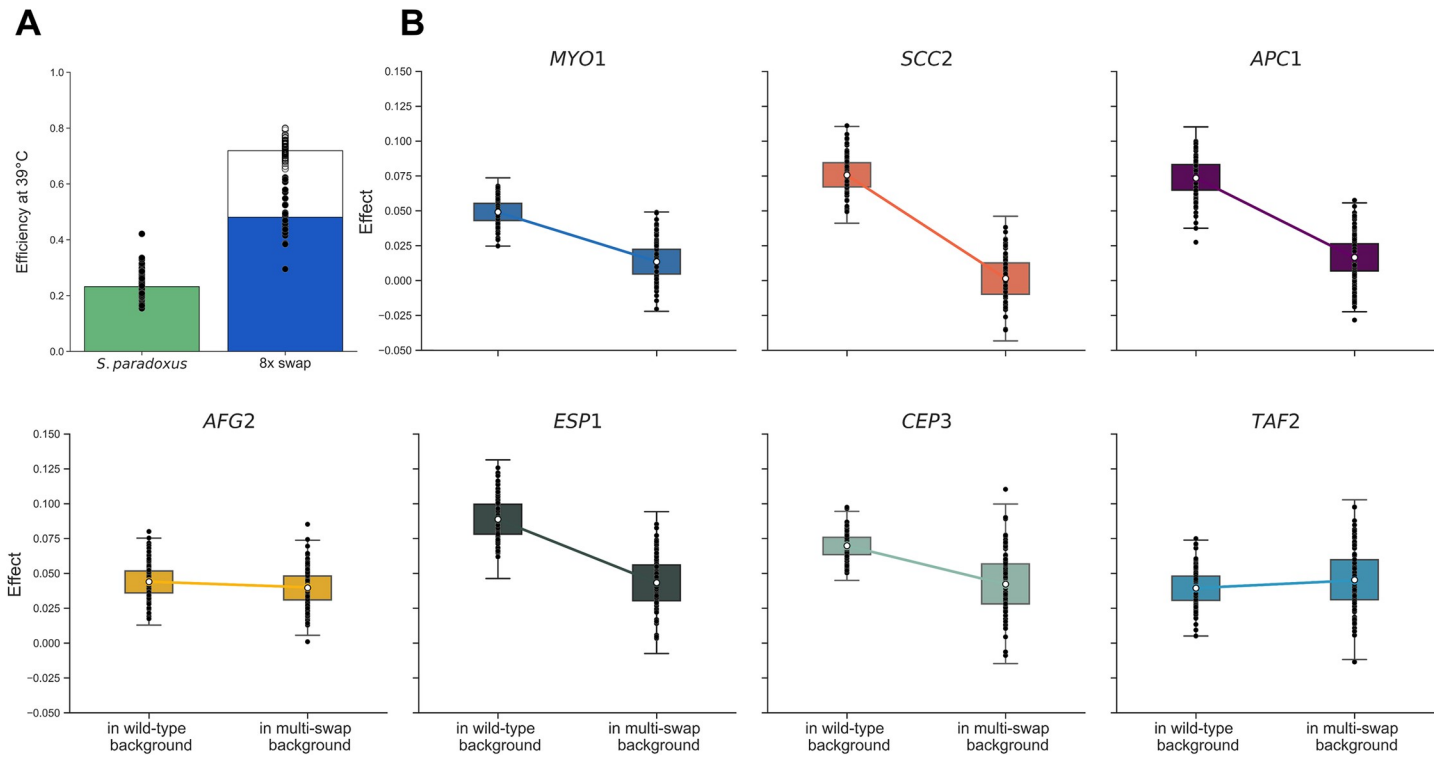


**Fig 2. Negative epistasis among *S. cerevisiae* alleles of thermotolerance loci.** (A) Solid bars report growth efficiency at 39˚C for, respectively, purebred *S. paradoxus* and the *S. paradoxus* strain harboring all eight thermotolerance loci from *S. cerevisiae* (8x swap). In the right column, the hollow extension reports the sum of the efficiencies at 39˚C of *S. paradoxus* strains harboring individual thermotolerance loci from *S. cerevisiae*, from S3 Fig. (B) In a given panel, the right-hand distribution shows the effect, on efficiency at 39˚C, of the *S. cerevisiae* allele of the indicated gene when introduced into a transgenic also harboring *S. cerevisiae* alleles of other genes, in the series of **Fig 1**. The left-hand distribution shows the analogous quantity when wild-type *S. paradoxus* was the background. Box and whisker format is as in **Fig 1**, except that for the sum of locus effects in (A), and for each component of (B), error was estimated by bootstrapping (see Methods).

https://doi.org/10.1371/journal.pgen.1009793.g002

was either below our detection limit or absent altogether in combination with *S. cerevisiae DYN1* and *MYO1* (encoding motor proteins; Figs 1 and 2B). Despite this potential case of masking epistasis, the remaining trend for beneficial effects by *S. cerevisiae* alleles as we built up the eight-locus strain was highly non-random (binomial $p = 0.03$). In no case did we observe a defect from swapping in an *S. cerevisiae* allele, meaning we had no evidence for sign epistasis in this system.

We also used our multi-genic strain panel, alongside single-gene transgenics in *S. paradoxus*, to compare *S. cerevisiae* allele-replacement effects across backgrounds. In most cases, a given thermotolerance gene from *S. cerevisiae* had less impact in the presence of other *S. cerevisiae* loci than when tested on its own in *S. paradoxus* (Fig 2B). This finding confirmed the negative (magnitude) epistasis between the *S. cerevisiae* alleles of thermotolerance genes that we had inferred with the eight-gene transgenic (Fig 2A). We noted that the damping of allelic effect by genetic background was most apparent at thermotolerance genes annotated in chromosome segregation/mitosis (*DYN1*, *MYO1*, *SCC2*, *APC1*, and *ESP1;* Fig 2B). By contrast, introducing the *S. cerevisiae* allele of *TAF2* or *AFG2*, involved in transcription and translation respectively, drove nearly the same benefit on its own in *S. paradoxus* and in the respective multi-swap chimera (Fig 2B).

Together, these genetic data characterize an example path toward thermotolerance of incremental advances from *S. cerevisiae* gene modules—most limiting each other's effects to some extent, but without frank deleterious consequences.

## Thermotolerance loci improve viability only during active growth

We next aimed to investigate cellular mechanisms of thermotolerance, using as a tool the strain with all eight of our focal genes from *S. cerevisiae* replaced into *S. paradoxus*. We focused on cell viability, as assayed by counts of colony-forming units (CFUs) from aliquots of liquid culture at 39˚C. In a first characterization of strain performance in growing cultures under this setup, *S. paradoxus* cells were much less viable than those of *S. cerevisiae*, across a range of warm temperatures (S4 Fig), as expected. We anticipated that *S. cerevisiae* alleles of our thermotolerance loci would rescue this phenotype, at least in part. This prediction bore out in our CFU assays from actively growing cultures: at 39˚C, the eight-gene transgenic survived 7-fold better than did its *S. paradoxus* progenitor (Fig 3A). An analogous test of wild-type *S. cerevisiae* revealed three logs higher viability than that of *S. paradoxus* during active growth at 39˚C (Fig 3A).

The poor performance of strains of *S. paradoxus* origin in the CFU assay (Fig 3A) was much bigger in magnitude than that seen in our measurements of biomass accumulation (Fig 1), in growing cultures. Such a discrepancy suggests that some cells with *S. paradoxus* genotypes managed to divide early in the heat treatment and then ultimately die, contributing at the end of the incubation to measured biomass but not viability. Qualitatively, however, both experiments led to the same conclusion: *S. cerevisiae* alleles of thermotolerance loci recapitulate part but not all of the advantage by *S. cerevisiae* relative to *S. paradoxus* during active growth at 39˚C. We detected no viability differences between strains during active growth at 28˚C (S5A Fig).

To gain insight into why *S. paradoxus* cells die at high temperature, we took account of the role in mitosis for most of our thermotolerance genes (Table 1). We hypothesized that failure of the *S. paradoxus* cell growth machinery was the proximal cause of death for this species at 39˚C. If so, we expected that the underlying alleles would not be a liability if cells did not enter the cell cycle in the first place. As a test of this notion, we retooled our viability assay to start by incubating a liquid culture at a permissive temperature until it reached stationary phase (when nutrients are exhausted and cell division arrests). We then switched these non-growing

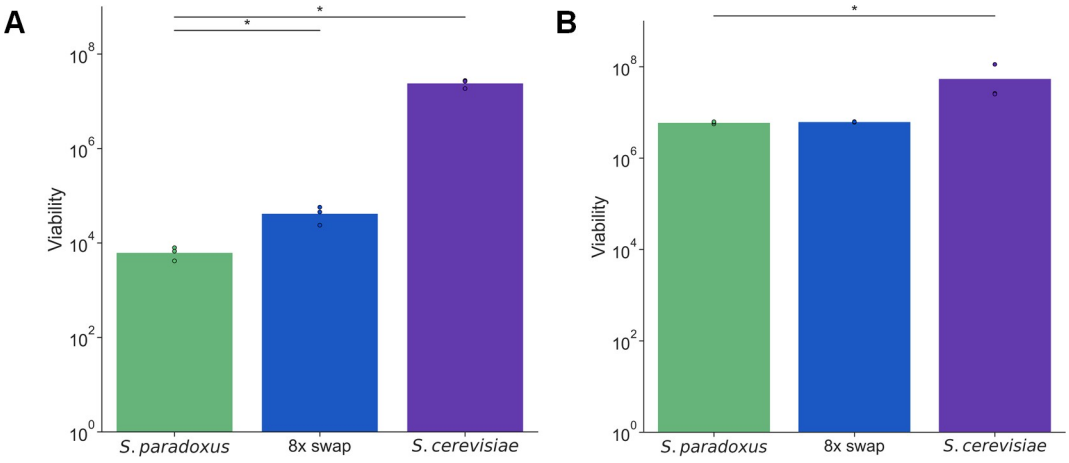


**Fig 3. *S. cerevisiae* alleles of thermotolerance loci jointly improve heat survival during growth but not in stationary phase.** In a given panel, each column reports viability after heat treatment of the wild-type of the indicated species, or the *S. paradoxus* strain harboring eight thermotolerance loci from *S. cerevisiae* (8x swap). The *y*-axis reports the number of colonies formed on solid medium from 1 mL of heat-treated liquid culture in (A) logarithmic growth or (B) stationary phase, normalized by turbidity. Points and bar heights report individual biological replicates and their means, respectively. *, Wilcoxon $p \leq 0.05$.

https://doi.org/10.1371/journal.pgen.1009793.g003

cultures to 39˚C, and finally took aliquots for assays of CFUs. The results revealed that, when exposed to heat as a stationary-phase culture, *S. paradoxus* survived nearly as well as did *S. cerevisiae* (Fig 3B), in contrast to the many logs of difference between the species during active growth (Fig 3A). Likewise, transgenesis of our eight thermotolerance genes had no impact on high temperature survival in stationary phase (Fig 3B). Viability experiments on stationary-phase cultures at 28˚C also found no difference between strains (S5B Fig).

These viability data show that the thermotolerance defect of *S. paradoxus* alleles from our eight-gene transgenic strain only manifests in actively growing cells, consistent with the hallmarks of cell cycle breakdown seen in microscopy assays of *S. paradoxus* at 39˚C [39]. Together, our results support a model in which passage through mitosis itself is lethal at high temperature for *S. paradoxus*, whereas cells in an arrested state are protected from damage and death. *S. cerevisiae*, meanwhile, grows and divides successfully at 39˚C, owing in part to its thermotolerant mitotic genes.

### An evolutionary tradeoff in tolerance of extreme temperatures

Given that *S. cerevisiae* is unique within its clade for its ability to grow at high temperatures, we anticipated that this trait could have evolved as part of a tradeoff, and that cold tolerance would be a logical potential opposing character. Consistent with this picture, we observed generally better cold resistance across a panel of wild *S. paradoxus* relative to environmental isolates of *S. cerevisiae* (S6 Fig). No such difference is detectable at 28˚C [39]. We reasoned that thermotolerance alleles at our eight focal genes could contribute to the poor growth by *S. cerevisiae* in the cold. Indeed, our eight-fold transgenic strain grew significantly worse than did wild-type *S. paradoxus* at 4˚C (Fig 4). With respect to biomass accumulation, this strain recapitulated 15% of the divergence between the wild-type species at 4˚C—paralleling the analogous quantity at 39˚C (Fig 1), and establishing antagonistic pleiotropy by *S. cerevisiae* alleles at our genes of interest.

We next addressed the genetic architecture of cold sensitivity, again focused on our eight thermotolerance loci. In tests of marginal effects by each of these genes individually, the *S. cerevisiae* allele of *DYN1* (encoding the dynein heavy chain) reduced biomass accumulation markedly at 4˚C when introduced into *S. paradoxus* on its own; a number of other genes had smaller effects (S7 Fig). Likewise, of our combinatorial gene replacements, most grew only slightly worse than the single-gene *DYN1* swap at 4˚C (S8 Fig). This contrasted with the stair-step-like trend of increasing thermotolerance as *S. cerevisiae* alleles were stacked in the *S. paradoxus* background (Fig 1). We conclude that, with respect to our focal genes, the genetic mechanisms of heat and cold tolerance do not strictly parallel each other, and that antagonistic pleiotropy between the temperatures is most salient for a single locus, *DYN1*.

In viability assays during growth at 39˚C, we had found robust divergence in survival between *S. cerevisiae* and *S. paradoxus*, as well as survival effects of variation at our thermotolerance loci (Fig 3A). It remained an open question whether the genetics of cold tolerance would have effects on cell death. In viability assays we saw very little difference between *S. cerevisiae*, *S. paradoxus*, and our eight-gene transgenic in the *S. paradoxus* background, in terms of CFUs after incubation at 4˚C (S9 Fig). This result underscores the difference in mechanism between cryotolerance and thermotolerance in this system, and establishes that *S. cerevisiae* alleles (at thermotolerance loci and others) slow growth in the cold rather than killing cells outright.

## Discussion

Evolution often uses variants at genes scattered throughout the genome to build an adaptive trait. The complete set of these loci, once in hand, can reconstitute the trait in an exogenous

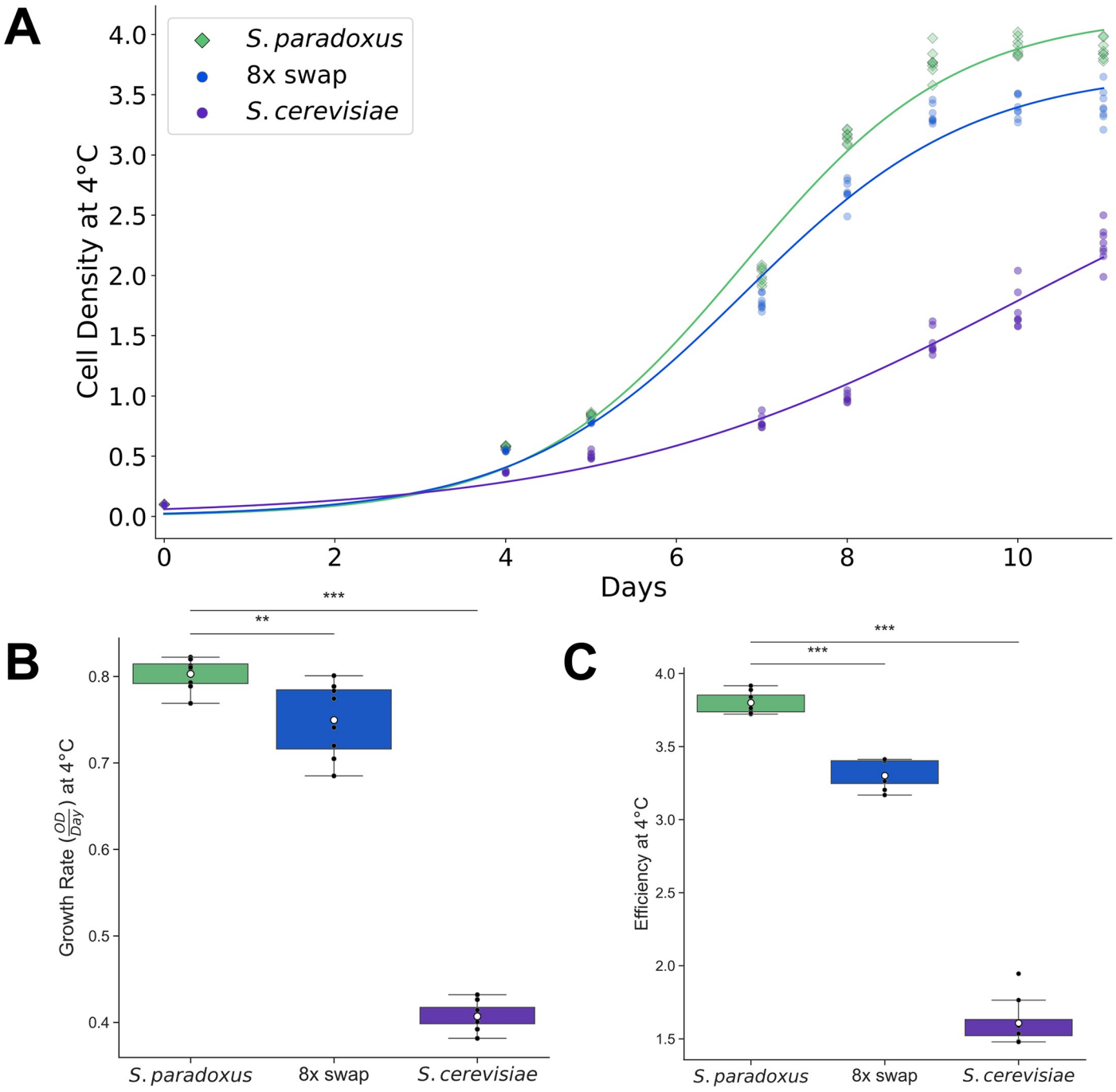


**Fig 4. *S. cerevisiae* alleles of thermotolerance loci jointly compromise growth in the cold.** (A) Each trace reports a timecourse of growth at 4˚C of the wild-type of the indicated species, or the *S. paradoxus* strain harboring eight thermotolerance loci from *S. cerevisiae* (8x swap). For a given strain, points on a given day report biological replicates; lines report the average fit from a logistic regression across replicates (S2 Table). (B) The *y*-axis reports growth rate, in units of cell density (optical density, OD) per day, from the average logistic fit of the timecourse in (A) for the indicated strain. (C) The *y*-axis reports, for day 10 of the timecourse in (A) for the indicated strain, growth efficiency, the cell density after a 10-day incubation at 4˚C as a difference from the starting density. In (B) and (C), points report individual biological replicates. Box and whisker format is as in Fig 1. ** and ***, Wilcoxon $p \leq 0.004$ and $p \leq 0.0005$, respectively.

https://doi.org/10.1371/journal.pgen.1009793.g004

background, which is the ultimate goal for many biomedically and industrially relevant characters. Along the way, the underlying genes can shed light on the process by which a trait arose, which may involve events from millions of years ago. In this work, we have used

thermotolerance, a putatively adaptive, fitness-relevant character [39,40], to explore genetic, biological, and evolutionary mechanisms of adaptation.

Introducing eight unlinked genes from *S. cerevisiae* into *S. paradoxus*, we reconstituted ~15% of the difference in thermotolerance between the respective purebred species. Much of the architecture for this trait thus remains unmapped, likely due in part to limitations of coverage and power in our original reciprocal hemizygosity scan [39], and to its restriction to the nuclear genome. Incisive experiments have established the role of mitotype in temperature tolerance as it differs between *S. cerevisiae* and either *S. paradoxus* or farther-diverged species of the complex, *S. uvarum* and *S. eubayanus* [42–45]. These mitochondrial variants presumably make up much of the heritability not accounted for by our current gene set. And *S. cerevisiae* alleles of the nuclear-encoded genes that we study here could well depend on the *S. cerevisiae* mitochondrial genome for their full effect.

In our focus on nuclear-encoded thermotolerance factors, we found that most *S. cerevisiae* alleles improved high-temperature growth, when tested on their own in *S. paradoxus* or in a chimeric multi-swap background. In principle, these effects could be limited by partial incompatibilities in *S. paradoxus*. That is, a given gene could have made an even bigger contribution to thermotolerance in the presence of other functional partners from *S. cerevisiae*. Even in such a case, the qualitative conclusion from our own data would remain: *S. cerevisiae* alleles mostly help and do not hurt at high temperature, alone or combined. This profile provides an intriguing contrast to the sign epistasis often detected between adaptive amino acid changes within any one protein, as they boost fitness in some combinations and compromise it in others [46,47]. Since we have not surveyed all possible subsets of our mapped thermotolerance genes, and more remain unidentified, we cannot rule out the possibility of toxic interactions at high temperature between some *S. cerevisiae* versions of unlinked loci when they come together. That said, our thermotolerance data as they stand conform to the idea that combining adaptive variants across unlinked sites will be less constrained than, say, repacking a protein [19]. This model is especially compelling in the search to understand evolutionary dynamics in sexual systems. If a gene module can recombine into most backgrounds and confer a benefit, it would speed the advance toward fitness of the population as a whole.

We found that the magnitude of the phenotypic effect of our focal genes depended on genetic background. For our analyses of epistasis, we focused on thermotolerance, under the assumption that this trait or its correlates have mattered for the fitness of *S. cerevisiae* in the environment, and that genetic interactions could have been at play during its evolution. We found ample evidence for negative epistasis, with the *S. cerevisiae* alleles of some of our unlinked loci obscuring the thermotolerance effects of others, in replacements into *S. paradoxus*. Negative epistasis has been a linchpin of classical genetic studies placing unlinked loss-of-function mutants in pathways [48,49], and their genomic equivalent, reverse-genetic double-mutant screens [50–53]. Negative epistasis also features in the polygenic architectures of putatively neutral and disease traits that vary in populations [54–56]. Our thermotolerance system complements these scenarios, in that we focus on alleles that act as gains of function, at least at high temperature [39]. Under the latter condition, we detected the most marked negative epistasis among thermotolerance genes with annotations in chromosome segregation and cell division. We can speculate that the *S. cerevisiae* allele at any such locus, as it rescues one aspect of mitosis at 39˚C, also pulls up the function of other parts of the mitotic machinery to some extent, *e.g.* by stabilizing heteromeric protein complexes. *S. cerevisiae* alleles of additional genes, introduced into such a background, would make less dramatic improvements to the phenotype than would be expected from their respective single-gene allele-swap strains.

Importantly, a sizeable literature has described negative epistasis between unlinked adaptive loci in laboratory evolution experiments, especially in microbes [7,21–29,57], where in some

studies, suites of unlinked variants have been validated in terms of effects on fitness [30,31]. A chief emphasis here has been on evolutionary dynamics, in that negative epistatic interactions limit the availability of mutational steps with big fitness effects that would otherwise speed adaptation [46,47]. This principle plays out in part through diminishing-returns epistasis [7,58], the difficulty of improving the fitness of somewhat-fit backgrounds, which can be explained by heightened susceptibility of fast-growing strains to pleiotropic effects of new mutations [59]. Though the latter has been a landmark of the recent literature, we do not consider it an immediately relevant model for our own data, because we work with backgrounds that perform very poorly at 39˚C. In more advanced stages of an allele-swap progression, which would reconstitute more of the yeast thermotolerance phenotype, we would expect genes to interact under the diminishing-returns mechanism.

Along with our insights into the genetics of thermotolerance, we discovered a cold resistance defect in *S. cerevisiae* relative to *S. paradoxus*, complementing previous temperature profiling using other assays across the genus [36,38]. We found that pro-thermotolerance alleles at our focal genes contribute to this character, most notably *DYN1*, which elicited the most dramatic drop in cold resistance when tested on its own in *S. paradoxus*, and overshadowed the effects of other loci in multi-gene swap backgrounds. This echoes the known breakdown of *S. cerevisiae DYN1* protein function below 8˚C, as distinguished from the mammalian ortholog [60]; additional deleterious effects could also manifest in conditions other than those we study here. The emerging picture from our work and that of others is that the evolution of thermotolerance in *S. cerevisiae* required, at least in part, the sacrifice of the ability to deal with cold. The tradeoff would have involved *DYN1* and its modifiers as well as mitochondrial genes, whose *S. cerevisiae* alleles are known to boost heat resistance and compromise cold growth [42–45]. And yet such a tradeoff need not be the whole evolutionary story. Some of the architecture of *S. cerevisiae* cold sensitivity could have arisen under other selective forces altogether. We can envision, for example, some degree of relaxed selection on cold tolerance in the *S. cerevisiae* ancestor, later in its evolution after commitment to a niche as a high-temperature specialist. Under one compelling model [61], supported by ethanol growth data [62,63], *S. cerevisiae's* more particular niche would have been as an avid glucose fermenter, with the resulting heat and ethanol both helping to kill off microbial competitors. Whether this or some other scenario proves to be the right description of *S. cerevisiae* ecology, our results attest to the complexity of the challenge faced by evolution, as it built the traits that define this species.

## Methods

### Strain construction

Strains used in this work are listed in S3 Table. To study combinations of *S. cerevisiae* alleles in an *S. paradoxus* background, we used as the latter the wild-type homozygous diploid *S. paradoxus* Z1, originally isolated from tree bark in England [41]. We used our CRISPR/Cas9 method [39], essentially as described but with slight modifications detailed below, to replace both copies of a given thermotolerance locus, at the endogenous location, with the allele from *S. cerevisiae* DBVPG1373, a soil isolate from the Netherlands [41]. To build the eight-gene transgenic, we started with the single-gene transgenic in the Z1 background harboring the *S. cerevisiae* allele of *DYN1* from [39]. We introduced *S. cerevisiae* alleles at additional genes in an iterative series of transformations; after each, we cultured an isogenic stock from a single colony for Sanger sequence confirmation and storage, and, where appropriate, we used this stock as input into the next transformation.

A given transformation involved donor DNA and constructs encoding guide RNAs for Cas9 to target replacement of the *S. paradoxus* allele with that from *S. cerevisiae* at either one

or two loci, which Sanger sequencing then verified to be successful at one or both. For each locus we used designs of guide RNAs from [39] that targeted, for double-strand breaks, the endogenous Z1 allele by Cas9; one guide targeted a site ~1000bp upstream of the coding start of the gene of interest (or the 3' end of the closest upstream gene) in the Z1 genome and the other guide targeted a site near the coding stop. Cas9 editing proceeded as described [39]. Briefly, for each transformation step of strain construction, one or two guide RNA pairs, targeting one or two loci respectively, were cloned into plasmid pBC712, which also encodes *Streptococcus pyogenes* Cas9. Next, DNA to serve as a repair template was generated for each relevant locus, via PCR from *S. cerevisiae* DBVPG1373, with 90bp primers that contained 70bp of sequence homologous to *S. paradoxus* Z1 on each side of the amplified DNA product. Finally, plasmid and repair template were transformed into the Z1 descendant as described [39] at a ratio of 0.3 to 3.5 based on the length of the donor DNA, equivalent to $10^{12}$ dsDNA molecules for 10 μg of plasmid. Putative transformants were purified and sequence-verified.

## Growth assays

Measurements of biomass accumulation (growth efficiency) at 39˚C in Fig 1 were done essentially as described [39] with modifications as follows. For a given day's worth of experiments, wild-type *S. paradoxus* Z1 and one or more other strains of interest were streaked onto a yeast peptone dextrose (YPD) plate from a -80˚C freezer stock and incubated at 28˚C for 2 days. 2–8 colonies of a given strain were each inoculated separately in 5mL of liquid YPD and grown for 24 hours at 28˚C with shaking at 200rpm to saturation; we refer to the cultures at this stage as pre-cultures. Each such replicate pre-culture was back-diluted into 10mL of YPD to achieve an $OD_{600}$ of 0.05; incubated at 28˚C until it reached an $OD_{600}$ of 0.4–0.8; back-diluted again to achieve an $OD_{600}$ of 0.1; and then incubated for 24 hours at 39˚C. We tabulated the difference in $OD_{600}$ between the final and initial timepoints across this 24-hour incubation for each culture. This procedure, from streaking on solid medium through inoculation, heat treatment, and biomass measurement, was repeated at least four times for each strain in the analysis of Fig 1. The resulting vector of biomass measurements across all replicates from all days for each strain was compared to that for each other strain with a one-tailed Wilcoxon test in S1 Table. Multiple testing was corrected for using the Benjamini-Hochberg method.

Measurements of biomass accumulation at 28˚C in S1 Fig were done as described [39]. Strains were streaked on solid plates and one colony per strain was pre-cultured in liquid at 28˚C as above. Each such saturated pre-culture was back-diluted to achieve an $OD_{600}$ of 0.05 and grown for an additional 5.5 hours at 28˚C until it reached logarithmic phase. We transferred cells from each such pre-culture, and YPD, to five replicate wells of a 96-well plate, with volumes sufficient to yield a total volume of 150 μL per well at an $OD_{600}$ of 0.02. The plate was covered with a gas-permeable membrane (Sigma) and incubated with orbital shaking in an M200 plate reader (Tecan, Inc.) at 28˚C for 24 hours. We tabulated the difference in $OD_{600}$ between the final and initial timepoints across this 24-hour incubation for each replicate culture. The vector of these replicate measurements for each strain was compared to that from *S. paradoxus* with a two-tailed Wilcoxon test. Multiple testing was corrected for using the Benjamini-Hochberg method.

For measurements of biomass accumulation at 37˚C—39˚C in S2 Fig, strains were streaked, and three colonies of a given strain were pre-cultured in liquid as above. Each such replicate liquid culture was back-diluted into 10mL of YPD to achieve an $OD_{600}$ of 0.05; incubated at 28˚C until it reached an $OD_{600}$ of 0.4–0.8; back-diluted again to $OD_{600}$ of to achieve an $OD_{600}$ of 0.1; and then incubated for 24 hours at the temperature of interest. We tabulated the difference in $OD_{600}$ between the final and initial timepoints across this 24-hour incubation for each

replicate culture. The vector of these replicate measurements for each strain at a given temperature was compared to that from *S. paradoxus* with a one-tailed Wilcoxon test. In S2 Fig, lines are the result of a polynomial regression on the points, created using Seaborn's regplot in Python 3.7.

For measurements of growth at 4˚C in Figs 4 and S6–S8, for a given day's worth of experiments, strains were streaked on solid plates and three to eight colonies per genotype, respectively, were pre-cultured in liquid, each as an independent biological replicate, as above. After the second back-dilution, each liquid culture was incubated for 11 days at 4˚C in a rotating shaker at maximum speed in a cold room. The $OD_{600}$ was measured on days 0, 4, 5, 7, 8, 9, 10, and 11, and also on day 6 for S6–S8 Figs. To measure biomass accumulation (growth efficiency) we tabulated the difference in $OD_{600}$ between the final and initial timepoints across this 11-day incubation for each replicate culture. Two such days' worth of experiments were carried out for each strain in S7 and S8 Figs, and one in Figs 4 and S6. We collated the measurements from all replicate culture measurements across all days for a given strain and compared each transgenic against *S. paradoxus* with a one-tailed Wilcoxon test. Separately, we fit a logistic curve to the timecourse measurements for each replicate using Scipy's curve_fit function as a part of Scipy's optimize package (Python 3.7). Bounds for the parameters of the logistic equation (the carrying capacity, growth rate, and time to half-maximal growth) were constrained to the range -1.0 to 10.0, and the Trust Region Reflective algorithm was used to find the best fit. We collated the growth rate estimates from all replicate culture measurements across all days for a given strain and compared each transgenic against *S. paradoxus* with a one-tailed Wilcoxon test. Multiple testing was corrected for using the Benjamini-Hochberg method.

## Viability assays

For the survey of viability phenotypes at high temperatures across environmental isolates in S4 Fig, strains were streaked out and four colonies of each were pre-cultured in liquid as for 39˚C growth above, except that the initial pre-culture to achieve saturation lasted 48 hours. Each pre-culture was back-diluted into 10 mL of YPD to reach an $OD_{600}$ of 0.05 and then cultured for 24 hours at the temperature of interest (35˚C—38˚C). The $OD_{600}$ at the end of this timecourse was measured for each such replicate culture. Then to measure viability for each, we diluted aliquots from the culture in a 1:10 series and spotted 3μL of each dilution for growth on a solid YPD plate. After incubation at 28˚C for two days, we used the dilution corresponding to the most dense spot that was not a lawn for the final report of viability: we counted the number of colonies in each of the two technical replicate spots, formulated the number of colony-forming units per mL of undiluted culture (CFU/mL), and divided this ratio by the $OD_{600}$ we had measured at the end of the liquid timecourse, to account for differences in the number of dead cells that contribute to the latter. At a given temperature, the vector of viability measurements across all replicate liquid cultures for all *S. cerevisiae* strains was compared to that for all *S. paradoxus* strains with a one-tailed Wilcoxon test.

For the comparison of viability between strains during log-phase growth at 39˚C in Fig 3A, strains were streaked out and three colonies of each were pre-cultured at 28˚C, back-diluted, and cultured at 39˚C, as for the 39˚C growth assays above. After 24 hours of incubation at 39˚C, for each such replicate culture, spotting of dilutions and colony counting to yield $CFU/mL/OD_{600}$ for each replicate liquid culture was done as above, except that we used two technical replicate spotting assay replicates for each culture, taking the average across them as the final report of viability. The vector of these viability measurements across replicates for a given strain was compared to that from *S. paradoxus* with a one-tailed Wilcoxon test.

For the comparison of viability between strains in stationary phase at 39˚C in Fig 3B, strains were streaked out and three colonies of each were pre-cultured at 28˚C as for the 39˚C growth assays above, except that that the initial pre-culture to achieve saturation lasted 72 hours. Each such replicate culture was then incubated (without back-dilution) at 39˚C for 24 hours, after which spotting, colony counting, and statistical testing were as for Fig 3A.

For the comparison of viability between strains during log-phase growth at 28˚C in S5A Fig, strains were streaked out and four colonies of each were pre-cultured at 28˚C and back-diluted as for the 39˚C growth assays above; each back-diluted replicate culture was incubated at 28˚C for 24 hours, after which spotting and colony counting was as above. For the comparison of viability between strains in stationary phase at 28˚C in S5B Fig, strains were streaked out as above, and three colonies of each were inoculated into liquid YPD at 28˚C and incubated for 96 hours, after which spotting, colony counting, and statistical testing were as for Fig 3A, except that two-sided Wilcoxon tests were performed.

For the comparison of viability between environmental strains during log-phase growth at 4˚C (S6 Fig), aliquots from cultures set up for cold growth assays (see above) were taken at day 8 of the cold timecourse for spotting, colony counting, and statistical testing as for Fig 3A.

## Epistasis analysis

For Fig 2A, we calculated the growth phenotype at 39˚C of the strain harboring all eight *S. cerevisiae* loci in the *S. paradoxus* background as expected under a model of independent locus effects as follows. We first tabulated the mean growth efficiency at 39˚C of each isogenic strain in turn with just one gene swapped in from *S. cerevisiae* and the analogous mean for *S. paradoxus*, and took the difference between them, representing the mean effect of the respective swap; we then summed the latter effect values across all eight loci. Error was estimated by bootstrapping as follows. For each locus, we generated a random sample of the replicate measurements of the growth efficiency of the respective swap strain at 39˚C with replacement, and took the mean; we calculated an analogous mean from a random sample of replicates of the *S. paradoxus* wild-type; and we took the difference between these means, representing one bootstrapped estimate of the effect of the swap. We then took the sum of such effects across all loci, representing one bootstrap's worth of the estimate of the eight-gene transgenic's phenotype under the additive model. We repeated this procedure 10,000 times to set up a distribution of the estimated sums in Fig 2A, showing 100 randomly chosen points to minimize figure complexity.

For a given panel of Fig 2B, the left-hand white point on the plot reports the mean effect of the *S. cerevisiae* allele of the respective gene when swapped alone into *S. paradoxus*. For this we tabulated the mean growth efficiency at 39˚C of this single-gene transgenic across all replicates and the analogous mean across all replicates of *S. paradoxus*, and took the difference between them. For error estimates, we generated a random sample of the replicate measurements of the growth efficiency of the respective swap strain at 39˚C with replacement, and took the mean; we calculated an analogous mean from a random sample of replicates of the *S. paradoxus* wild-type; and we took the difference between these means, representing one bootstrapped estimate of the effect of the swap. We repeated this procedure 10,000 times to set up a distribution of the estimated effect values in Fig 2B, showing 100 randomly chosen points to minimize figure complexity. The right-hand white point on the plot reports the mean effect of the *S. cerevisiae* allele of the respective gene when swapped into a multi-genic strain of the *S. paradoxus* background in the series culminating in the eight-fold transgenic, in the order of Fig 1. Call the strain before and after the replacement of the gene of interest *X-1* and *X*, respectively; we tabulated the mean growth efficiency at 39˚C across all replicates of strain *X* and the analogous

quantity for strain *X-1*, and took the difference between them. Error was estimated by bootstrapping as above.

## Supporting information

**S1 Table. Statistical analyses of growth at 39˚C and 28˚C.** (A) Each cell reports the results of a one-sided Wilcoxon test comparing growth efficiency at 39˚C between the indicated strains, in Fig 1 of the main text. Multiple testing was corrected for using the Benjamini-Hochberg method. (B) Data are as in A except that analysis was of growth efficiency at 28˚C from S1 Fig, and two-sided Wilcoxon tests were applied.
(TIF)

**S2 Table. Parameters used in regressions.** Each row reports fitted values of the indicated parameters from the polynomial regression (S2 Fig) or logistic regression (all other figures) of growth measurements of the indicated strain for the indicated figure. For the logistic regression, K, R, and $x_0$ are the carrying capacity, logistic growth rate, and the sigmoidal midpoint, respectively.
(XLSX)

**S3 Table. Strains used in this study. A.** Wild-type diploid strains, including those used as parents of allele-replacement transgenesis; SGRP, the Saccharomyces Genome Resequencing Project, version 2. **B.** Purebred allele replacement strains in *S. paradoxus* Z1 diploid homozygote backgrounds. In genotype notes, *e.g.*, in an *S. paradoxus* background, ΔYFG(-X to +Y):: scYFG(-Z to +W) indicates that in *S. paradoxus* Z1, bases -X to +Y from both homologs of gene YFG have been removed and replaced by bases -Z to +W of the allele of YFG from the indicated *S. cerevisiae* strain. Positive coordinates count in the 5' to 3' direction from the start codon (+1 corresponds to the A in the ATG), and negative coordinates count in the 3' to 5' direction from the start codon (-1 corresponds to the base directly 5' of the ATG). In cases where the replacement extended into a region of 100% conservation between species, the position of the last divergent nucleotide is shown.
(XLSX)

**S1 Fig. Allelic variation at thermotolerance loci has little growth impact at 28˚C.** Data and symbols are as in Fig 1 of the main text except that growth was measured at 28˚C. Statistical analyses are reported in S1B Table.
(TIF)

**S2 Fig. *S. cerevisiae* alleles of thermotolerance loci jointly improve growth at temperatures from 37˚C—39˚C.** In a given panel, each trace reports growth efficiency, the cell density after a 24-hour incubation at the indicated temperature as a difference from the starting density, of the wild-type of the indicated species or the *S. paradoxus* strain harboring eight thermotolerance loci from S. cerevisiae (8x swap). Lines are the result of a polynomial regression on the points (S2 Table). *, Wilcoxon $p \leq 0.0404$.
(TIF)

**S3 Fig. *S. cerevisiae* alleles of thermotolerance loci individually improve growth at high temperature.** Data and symbols are as in the main panel of Fig 1 except that each column reports results from the indicated wild-type strain or a strain of *S. paradoxus* harboring the *S. cerevisiae* allele of the indicated single gene and the *y*-axis is log-scaled. All comparisons to *S. paradoxus* had one-sided Wilcoxon $p < 0.01$ after correction for multiple testing.
(TIF)

**S4 Fig. Environmental isolates of *Saccharomyces* spp. differ in heat survival.** Each cell reports viability after heat treatment of the indicated strain and species: the number of colonies formed on solid medium from 1 mL of heat-treated liquid culture in logarithmic growth, normalized by the turbidity of the latter. *S. paradoxus* Z1, N17, and A12 are isolates from UK, Russia, and Quebec, respectively; *S. cerevisiae* strains DBVPG1373, DBVPG1788, YPS128 are from the Netherlands, Finland, and Pennsylvania, respectively. Viability was different between species at Wilcoxon $p < 0.00002$ for all temperatures.
(TIF)

**S5 Fig. Allelic variation at thermotolerance loci has no impact on viability at 28˚C.** Data and symbols are as in Fig 3 of the main text except that liquid incubations were at 28˚C. In no case was the respective measurement for a given strain significantly different from the analogous quantity for *S. paradoxus* at two-sided Wilcoxon $p < 0.05$.
(TIF)

**S6 Fig. Environmental isolates of *Saccharomyces spp*. differ in ability to grow at 4˚C.** (A) Each trace reports a timecourse of growth at 4˚C of the wild-type of the indicated strain. For a given strain, points on a given day report biological replicates; lines report the average fit from a logistic regression across replicates (S2 Table). YPS128, a North American *S. cerevisiae* known to have recently acquired freeze-thaw resistance as a derived character distinct from the ancestral program [64], is shown in faint blue. (B) The *y*-axis reports growth rate, in units of cell density (optical density, OD) per day, from the average logistic fit of the timecourse in (A) for the indicated strain. (C) The *y*-axis reports, for day 10 of the timecourse in (A) for the indicated strain, growth efficiency, the cell density after a 10-day incubation at 4˚C as a difference from the starting density. In (B) and (C), Black points report individual biological replicates. White dots report means. Boxes span the interquartile range; whiskers are 1.5 times the interquartile range, and do not report outliers. Comparisons of growth rate and efficiency at 4˚C between *S. paradoxus* strains and *S. cerevisiae* strains yielded Wilcoxon $p \leq 0.00003$ and $p \leq 0.002$, respectively.
(TIF)

**S7 Fig. Growth effects at 4˚C of *S. cerevisiae* alleles of individual thermotolerance loci.** (A) Data and symbols are as in S3 Fig except that the *y*-axis reports growth efficiency after a 10-day incubation at 4˚C. (B) Data are as in (A) except that the y-axis reports growth rate, in units of cell density (optical density, OD) per day, from the average logistic fit of the timecourse for the indicated strain (S2 Table). *, corrected one-sided Wilcoxon $p \leq 0.05$.
(TIF)

**S8 Fig. Joint growth effects at 4˚C of *S. cerevisiae* alleles of subsets of thermotolerance loci.** (A) Data and symbols are as in the main panel of Fig 1 except that the y-axis reports growth efficiency after a 10-day incubation at 4˚C. (B) Data and symbols are as in (A) except that the y-axis reports growth rate, in units of cell density (optical density, OD) per day, from the average logistic fit of the timecourse for the indicated strain (S2 Table). * and **, corrected one-sided Wilcoxon $p \leq 0.05$ and 0.01 respectively.
(TIF)

**S9 Fig. Allelic variation at thermotolerance loci has little impact on viability at 4˚C.** Data and symbols are as in Fig 3A of the main text, except that liquid incubations were at 4˚C, and measurements were taken at day 8 of the growth timecourse. *, One-sided Wilcoxon $p \leq 0.05$.
(TIF)

## Acknowledgments

The authors thank Dmitri Petrov for motivating the analysis of the thermotolerance of stationary-phase cultures; Abel Duarte and Jeff Skerker for direction and advice with molecular biology; Carly Weiss and Jeremy Roop for other helpful discussions; and David Savage for his generosity with lab facilities and resources.

## Author Contributions

**Conceptualization:** Faisal AlZaben, Rachel B. Brem.

**Formal analysis:** Faisal AlZaben, Rachel B. Brem.

**Funding acquisition:** Melanie B. Abrams, Rachel B. Brem.

**Investigation:** Faisal AlZaben.

**Methodology:** Faisal AlZaben, Julie N. Chuong, Melanie B. Abrams.

**Project administration:** Rachel B. Brem.

**Resources:** Rachel B. Brem.

**Supervision:** Rachel B. Brem.

**Visualization:** Faisal AlZaben.

**Writing – original draft:** Faisal AlZaben, Rachel B. Brem.

**Writing – review & editing:** Faisal AlZaben, Julie N. Chuong, Melanie B. Abrams, Rachel B. Brem.

## References

1. Burke MK, Rose MR. Experimental evolution with Drosophila. Am J Physiol Regul Integr Comp Physiol. 2009; 296: R1847–1854. https://doi.org/10.1152/ajpregu.90551.2008 PMID: 19339679
2. Iranmehr A, Stobdan T, Zhou D, Zhao H, Kryazhimskiy S, Bafna V, et al. Multiple mechanisms drive genomic adaptation to extreme O2 levels in Drosophila melanogaster. Nat Commun. 2021; 12: 997. https://doi.org/10.1038/s41467-021-21281-6 PMID: 33579965
3. Pardo-Diaz C, Salazar C, Jiggins CD. Towards the identification of the loci of adaptive evolution. Methods Ecol Evol. 2015; 6: 445–464. https://doi.org/10.1111/2041-210X.12324 PMID: 25937885
4. Sella G, Barton NH. Thinking About the Evolution of Complex Traits in the Era of Genome-Wide Association Studies. Annu Rev Genomics Hum Genet. 2019; 20: 461–493. https://doi.org/10.1146/annurev-genom-083115-022316 PMID: 31283361
5. Castro JP, Yancoskie MN, Marchini M, Belohlavy S, Hiramatsu L, Kučka M, et al. An integrative genomic analysis of the Longshanks selection experiment for longer limbs in mice. eLife. 2019; 8. https://doi.org/10.7554/eLife.42014 PMID: 31169497
6. Chan YF, Marks ME, Jones FC, Villarreal G, Shapiro MD, Brady SD, et al. Adaptive evolution of pelvic reduction in sticklebacks by recurrent deletion of a Pitx1 enhancer. Science. 2010; 327: 302–305. https://doi.org/10.1126/science.1182213 PMID: 20007865
7. Kryazhimskiy S, Rice DP, Jerison ER, Desai MM. Microbial evolution. Global epistasis makes adaptation predictable despite sequence-level stochasticity. Science. 2014; 344: 1519–1522. https://doi.org/10.1126/science.1250939 PMID: 24970088
8. Linnen CR, Poh Y-P, Peterson BK, Barrett RDH, Larson JG, Jensen JD, et al. Adaptive evolution of multiple traits through multiple mutations at a single gene. Science. 2013; 339: 1312–1316. https://doi.org/10.1126/science.1233213 PMID: 23493712
9. Linnen CR, Kingsley EP, Jensen JD, Hoekstra HE. On the origin and spread of an adaptive allele in deer mice. Science. 2009; 325: 1095–1098. https://doi.org/10.1126/science.1175826 PMID: 19713521
10. Xie KT, Wang G, Thompson AC, Wucherpfennig JI, Reimchen TE, MacColl ADC, et al. DNA fragility in the parallel evolution of pelvic reduction in stickleback fish. Science. 2019; 363: 81–84. https://doi.org/10.1126/science.aan1425 PMID: 30606845

11. Anderson DP, Whitney DS, Hanson-Smith V, Woznica A, Campodonico-Burnett W, Volkman BF, et al. Evolution of an ancient protein function involved in organized multicellularity in animals. eLife. 2016; 5: e10147. https://doi.org/10.7554/eLife.10147 PMID: 26740169

12. Bridgham JT, Ortlund EA, Thornton JW. An epistatic ratchet constrains the direction of glucocorticoid receptor evolution. Nature. 2009; 461: 515–519. https://doi.org/10.1038/nature08249 PMID: 19779450

13. Escudero JA, Nivina A, Kemble HE, Loot C, Tenaillon O, Mazel D. Primary and promiscuous functions coexist during evolutionary innovation through whole protein domain acquisitions. eLife. 2020; 9. https://doi.org/10.7554/eLife.58061 PMID: 33319743

14. Finnigan GC, Hanson-Smith V, Stevens TH, Thornton JW. Evolution of increased complexity in a molecular machine. Nature. 2012; 481: 360–364. https://doi.org/10.1038/nature10724 PMID: 22230956

15. Lindsey HA, Gallie J, Taylor S, Kerr B. Evolutionary rescue from extinction is contingent on a lower rate of environmental change. Nature. 2013; 494: 463–467. https://doi.org/10.1038/nature11879 PMID: 23395960

16. Liu Q, Onal P, Datta RR, Rogers JM, Schmidt-Ott U, Bulyk ML, et al. Ancient mechanisms for the evolution of the bicoid homeodomain's function in fly development. eLife. 2018;7. https://doi.org/10.7554/eLife.34594 PMID: 30298815

17. Palmer AC, Toprak E, Baym M, Kim S, Veres A, Bershtein S, et al. Delayed commitment to evolutionary fate in antibiotic resistance fitness landscapes. Nat Commun. 2015; 6: 7385. https://doi.org/10.1038/ncomms8385 PMID: 26060115

18. Pillai AS, Chandler SA, Liu Y, Signore AV, Cortez-Romero CR, Benesch JLP, et al. Origin of complexity in haemoglobin evolution. Nature. 2020; 581: 480–485. https://doi.org/10.1038/s41586-020-2292-y PMID: 32461643

19. Toprak E, Veres A, Michel J-B, Chait R, Hartl DL, Kishony R. Evolutionary paths to antibiotic resistance under dynamically sustained drug selection. Nat Genet. 2011; 44: 101–105. https://doi.org/10.1038/ng.1034 PMID: 22179135

20. Weinreich DM, Delaney NF, Depristo MA, Hartl DL. Darwinian evolution can follow only very few mutational paths to fitter proteins. Science. 2006; 312: 111–114. https://doi.org/10.1126/science.1123539 PMID: 16601193

21. Aggeli D, Li Y, Sherlock G. Changes in the distribution of fitness effects and adaptive mutational spectra following a single first step towards adaptation. Nat Commun 2021; 12:5193. https://doi.org/10.1038/s41467-021-25440-7 PMID: 34465770

22. Blount ZD, Barrick JE, Davidson CJ, Lenski RE. Genomic analysis of a key innovation in an experimental Escherichia coli population. Nature. 2012; 489: 513–518. https://doi.org/10.1038/nature11514 PMID: 22992527

23. Bons E, Leemann C, Metzner KJ, Regoes RR. Long-term experimental evolution of HIV-1 reveals effects of environment and mutational history. PLoS Biol. 2020; 18: e3001010. https://doi.org/10.1371/journal.pbio.3001010 PMID: 33370289

24. Buskirk SW, Peace RE, Lang GI. Hitchhiking and epistasis give rise to cohort dynamics in adapting populations. Proc Natl Acad Sci U S A. 2017; 114: 8330–8335. https://doi.org/10.1073/pnas.1702314114 PMID: 28720700

25. Csilléry K, Rodríguez-Verdugo A, Rellstab C, Guillaume F. Detecting the genomic signal of polygenic adaptation and the role of epistasis in evolution. Mol Ecol. 2018; 27: 606–612. https://doi.org/10.1111/mec.14499 PMID: 29385652

26. Fisher KJ, Kryazhimskiy S, Lang GI. Detecting genetic interactions using parallel evolution in experimental populations. Philos Trans R Soc Lond B Biol Sci. 2019; 374: 20180237. https://doi.org/10.1098/rstb.2018.0237 PMID: 31154981

27. Good BH, McDonald MJ, Barrick JE, Lenski RE, Desai MM. The dynamics of molecular evolution over 60,000 generations. Nature. 2017; 551: 45–50. https://doi.org/10.1038/nature24287 PMID: 29045390

28. Johnson MS, Gopalakrishnan S, Goyal J, Dillingham ME, Bakerlee CW, Humphrey PT, et al. Phenotypic and molecular evolution across 10,000 generations in laboratory budding yeast populations. eLife. 2021; 10: e63910. https://doi.org/10.7554/eLife.63910 PMID: 33464204

29. Weber K, Eisman R, Morey L, Patty A, Sparks J, Tausek M, et al. An analysis of polygenes affecting wing shape on chromosome 3 in Drosophila melanogaster. Genetics. 1999; 153: 773–786. PMID: 10511557

30. Chou H-H, Chiu H-C, Delaney NF, Segrè D, Marx CJ. Diminishing returns epistasis among beneficial mutations decelerates adaptation. Science. 2011; 332: 1190–1192. https://doi.org/10.1126/science.1203799 PMID: 21636771

31. Khan AI, Dinh DM, Schneider D, Lenski RE, Cooper TF. Negative epistasis between beneficial mutations in an evolving bacterial population. Science. 2011; 332: 1193–1196. https://doi.org/10.1126/science.1203801 PMID: 21636772

32. Marcusson LL, Frimodt-Møller N, Hughes D. Interplay in the selection of fluoroquinolone resistance and bacterial fitness. PLoS Pathog. 2009; 5: e1000541. https://doi.org/10.1371/journal.ppat.1000541 PMID: 19662169

33. Neverov AD, Kryazhimskiy S, Plotkin JB, Bazykin GA. Coordinated Evolution of Influenza A Surface Proteins. PLoS Genet. 2015; 11: e1005404. https://doi.org/10.1371/journal.pgen.1005404 PMID: 26247472

34. Roop JI, Chang KC, Brem RB. Polygenic evolution of a sugar specialization trade-off in yeast. Nature. 2016; 530: 336–339. https://doi.org/10.1038/nature16938 PMID: 26863195

35. Gonçalves P, Valério E, Correia C, de Almeida JMGCF, Sampaio JP. Evidence for divergent evolution of growth temperature preference in sympatric Saccharomyces species. PloS One. 2011; 6: e20739. https://doi.org/10.1371/journal.pone.0020739 PMID: 21674061

36. Salvadó Z, Arroyo-López FN, Guillamón JM, Salazar G, Querol A, Barrio E. Temperature adaptation markedly determines evolution within the genus Saccharomyces. Appl Environ Microbiol. 2011; 77: 2292–2302. https://doi.org/10.1128/AEM.01861-10 PMID: 21317255

37. Sweeney JY, Kuehne HA, Sniegowski PD. Sympatric natural Saccharomyces cerevisiae and S. paradoxus populations have different thermal growth profiles. FEMS Yeast Res. 2004; 4: 521–525. https://doi.org/10.1016/S1567-1356(03)00171-5 PMID: 14734033

38. Hittinger CT. Saccharomyces diversity and evolution: a budding model genus. Trends Genet TIG. 2013; 29: 309–317. https://doi.org/10.1016/j.tig.2013.01.002 PMID: 23395329

39. Weiss CV, Roop JI, Hackley RK, Chuong JN, Grigoriev IV, Arkin AP, et al. Genetic dissection of interspecific differences in yeast thermotolerance. Nat Genet. 2018; 50: 1501–1504. https://doi.org/10.1038/s41588-018-0243-4 PMID: 30297967

40. Abrams MB, Dubin CA, AlZaben F, Bravo J, Joubert PM, Weiss CV, et al. Population and comparative genetics of thermotolerance divergence between yeast species. G3 GenesGenomesGenetics. 2021; jkab139. https://doi.org/10.1093/g3journal/jkab139 PMID: 33914073

41. Liti G, Carter DM, Moses AM, Warringer J, Parts L, James SA, et al. Population genomics of domestic and wild yeasts. Nature. 2009; 458: 337–341. https://doi.org/10.1038/nature07743 PMID: 19212322

42. Baker EP, Peris D, Moriarty RV, Li XC, Fay JC, Hittinger CT. Mitochondrial DNA and temperature tolerance in lager yeasts. Sci Adv. 2019; 5: eaav1869. https://doi.org/10.1126/sciadv.aav1869 PMID: 30729163

43. Hewitt SK, Duangrattanalert K, Burgis T, Zeef LAH, Naseeb S, Delneri D. Plasticity of Mitochondrial DNA Inheritance and its Impact on Nuclear Gene Transcription in Yeast Hybrids. Microorganisms. 2020; 8. https://doi.org/10.3390/microorganisms8040494 PMID: 32244414

44. Li XC, Peris D, Hittinger CT, Sia EA, Fay JC. Mitochondria-encoded genes contribute to evolution of heat and cold tolerance in yeast. Sci Adv. 2019; 5: eaav1848. https://doi.org/10.1126/sciadv.aav1848 PMID: 30729162

45. Špírek M, Poláková S, Jatzová K, Sulo P. Post-zygotic sterility and cytonuclear compatibility limits in S. cerevisiae xenomitochondrial cybrids. Front Genet. 2014; 5: 454. https://doi.org/10.3389/fgene.2014.00454 PMID: 25628643

46. Starr TN, Thornton JW. Epistasis in protein evolution. Protein Sci Publ Protein Soc. 2016; 25: 1204–1218. https://doi.org/10.1002/pro.2897 PMID: 26833806

47. Weinreich DM, Watson RA, Chao L. Perspective: Sign epistasis and genetic constraint on evolutionary trajectories. Evol Int J Org Evol. 2005; 59: 1165–1174. PMID: 16050094

48. Avery L, Wasserman S. Ordering gene function: the interpretation of epistasis in regulatory hierarchies. Trends Genet TIG. 1992; 8: 312–316. https://doi.org/10.1016/0168-9525(92)90263-4 PMID: 1365397

49. Roth FP, Lipshitz HD, Andrews BJ. Q&A: epistasis. J Biol. 2009; 8: 35. https://doi.org/10.1186/jbiol144 PMID: 19486505

50. Baryshnikova A, Costanzo M, Myers CL, Andrews B, Boone C. Genetic interaction networks: toward an understanding of heritability. Annu Rev Genomics Hum Genet. 2013; 14: 111–133. https://doi.org/10.1146/annurev-genom-082509-141730 PMID: 23808365

51. Shen JP, Zhao D, Sasik R, Luebeck J, Birmingham A, Bojorquez-Gomez A, et al. Combinatorial CRISPR-Cas9 screens for de novo mapping of genetic interactions. Nat Methods. 2017; 14: 573–576. https://doi.org/10.1038/nmeth.4225 PMID: 28319113

52. Tutuncuoglu B, Krogan NJ. Mapping genetic interactions in cancer: a road to rational combination therapies. Genome Med. 2019; 11: 62. https://doi.org/10.1186/s13073-019-0680-4 PMID: 31640753

53. Wong ASL, Choi GCG, Lu TK. Deciphering Combinatorial Genetics. Annu Rev Genet. 2016; 50: 515–538. https://doi.org/10.1146/annurev-genet-120215-034902 PMID: 27732793

54. Gusareva ES, Van Steen K. Practical aspects of genome-wide association interaction analysis. Hum Genet. 2014; 133: 1343–1358. https://doi.org/10.1007/s00439-014-1480-y PMID: 25164382

55. Mackay TFC. Epistasis and quantitative traits: using model organisms to study gene-gene interactions. Nat Rev Genet. 2014; 15: 22–33. https://doi.org/10.1038/nrg3627 PMID: 24296533

56. Ritchie MD. Finding the epistasis needles in the genome-wide haystack. Methods Mol Biol Clifton NJ. 2015; 1253: 19–33. https://doi.org/10.1007/978-1-4939-2155-3_2 PMID: 25403525

57. Tenaillon O, Rodríguez-Verdugo A, Gaut RL, McDonald P, Bennett AF, Long AD, et al. The molecular diversity of adaptive convergence. Science. 2012; 335: 457–461. https://doi.org/10.1126/science.1212986 PMID: 22282810

58. Wiser MJ, Ribeck N, Lenski RE. Long-term dynamics of adaptation in asexual populations. Science. 2013; 342: 1364–1367. https://doi.org/10.1126/science.1243357 PMID: 24231808

59. Johnson MS, Martsul A, Kryazhimskiy S, Desai MM. Higher-fitness yeast genotypes are less robust to deleterious mutations. Science. 2019; 366: 490–493. https://doi.org/10.1126/science.aay4199 PMID: 31649199

60. Hong W, Takshak A, Osunbayo O, Kunwar A, Vershinin M. The Effect of Temperature on Microtubule-Based Transport by Cytoplasmic Dynein and Kinesin-1 Motors. Biophys J. 2016; 111: 1287–1294. https://doi.org/10.1016/j.bpj.2016.08.006 PMID: 27653487

61. Goddard MR. Quantifying the complexities of Saccharomyces cerevisiae's ecosystem engineering via fermentation. Ecology. 2008; 89: 2077–2082. https://doi.org/10.1890/07-2060.1 PMID: 18724717

62. Herbst RH, Bar-Zvi D, Reikhav S, Soifer I, Breker M, Jona G, et al. Heterosis as a consequence of regulatory incompatibility. BMC Biol. 2017; 15: 38. https://doi.org/10.1186/s12915-017-0373-7 PMID: 28494792

63. Williams KM, Liu P, Fay JC. Evolution of ecological dominance of yeast species in high-sugar environments. Evol Int J Org Evol. 2015; 69: 2079–2093. https://doi.org/10.1111/evo.12707 PMID: 26087012

64. Will JL, Kim HS, Clarke J, Painter JC, Fay JC, Gasch AP. Incipient balancing selection through adaptive loss of aquaporins in natural Saccharomyces cerevisiae populations. PLoS Genet. 2010;6: e1000893. https://doi.org/10.1371/journal.pgen.1000893.